**American Journal of Applied Sciences and Engineering (AJASE)** | **ISSN** *2766-7596*
Published by ACADEMIC INK REVIEW | *https://airjournal.org/ajase*
12011 WestBrae Pkwy, Houston, TX 77031, United States
airjournals@gmail.com; enquiry@airjournal.org

# Investigation of the Experimental Correlation between Heat Treatment Parameter and Corrosion Behaviour of 718 Series Ni-Fe Superalloy in HCL Solution

**[1]Nwogbu, C. C, [2]Nwogbu, Paul U. and [3]Arum, Marcel O.**

**[1]Depatment of Metallurgical and Materials Engineering**
**[2,3]Department of Chemical Engineering**
**Enugu State University of Science and Technology, Enugu, Nigeria.**

| *Publication Process* | *Date* |
|---|---|
| *Received* | ***December 28th, 2020*** |
| *Accepted* | ***January 11th, 2021*** |
| *Published* | ***January 15th, 2021*** |

**ABSTRACT**

*The correlation between heat treatment parameter and corrosion behavior of 718 Ni-Fe superalloy was investigated in H2SO4 solution. Spark plasma sintering (SPS) was used in producing the samples which was then heat treated at temperatures of 800OC and 10000C and time of 1 and 2 hours for each temperature. Electrochemical studies were carried out in H2SO4 medium, using potentiodynammic anodic polarization techniques. It was observed from the results that the heat-treated alloy showed better corrosion resistance than the untreated alloy. Heat treatment temperature and time have great influences on the corrosion behavior and morphology of the alloy. An optimal protection efficiency of 55.29% was given by sample heat treated at 8000C for 2hours.it has been established that heat treatment can be used to improve the corrosion resistance of the alloy.*

***Keywords:*** *Ni-Fe alloy, Microstructure, Corrosion and Heat Treatment*

**Introduction**

Nickel-Iron base alloys appear to be a promising alternative to austenitic stainless steels because of their better corrosion resistance, thermal conductivity and mechanical properties. Using these alloys, complex processes and waste streams can be handled safely due to their high corrosion resistance (Viswanathan et al., 2005; Locq, Walder, Marty, Caron 2000). Theses alloys possess higher tolerance for alloying elements in solid solution than stainless steels and other iron base alloys (Wlodek, Kelly & Alden, 1992). The good metallurgical stability of the nickel base alloys makes them a better alternative to stainless steel (Soucail, Marty, Octor, 1996; Khadiah, 2015). Owing to the excellent mechanical and physical properties, nickel base superalloys are extensively employed in nuclear power plants (Wesley & Copson, 1946).

INCONEL 718 alloy can be fabricated with ease, combined with good tensile, fatigue, creep, and rupture strength, have resulted in its use in a wide range of applications. It has been widely used in the aircraft industry due to its high-strength, corrosion-resistant and excellent mechanical properties at elevated temperatures (Li et al., 2018). INCONEL718 is strengthened mainly by the nano-scale ɣ" (Ni3Nb) and ɣ' (Ni3(Al, Ti) phases. The ɣ" phase has a disc shape with a body centered tetragonal (bct) structure (Calandri et al., 2018; Zhang et al., 2018). The ɣ' phase has a cubic (fcc) structure and precipitates as a cube-to-cube relationship with the matrix (Ma et al., 2019). There will be more ɣ" than ɣ' in the alloy due to its composition. The ɣ" phase is metastable and can transform into the δ (Ni3Nb) phase at high temperatures, (Lin et al., 2019, Sano et al., 2013). Adequate amounts of δ phases at grain boundaries can refine the grain sizes and improve the resistance to grain boundary creep fracture, (Lyu, et al., 2019; Deng; Moverare; Peng; Söderberg, 2017).

The high temperature performance of the Ni-base superalloy Superni-75 has been evaluated under cyclic conditions for 1000hinreal service environment of the waste incinerator based upon medical waste as fuel. The performance has been characterized via surface morphology, phase composition and element concentration using the combined techniques of XRD, SEM/EDX, BSEI and EPMA. Initially, due to chlorine-based corrosion attack on the Superni-75 alloy, there was inner penetration of the corrosive species. However, with the growth of a thin Cr2O3 interface layer along the scale/surface boundary, the performance of the alloy improved against the attack by the flue gases in the real service conditions of the medical waste incinerator. Boiler tubes made of Superni-75 were estimated to have an erosion-corrosion rate of about 65 mils/year.

Paula et al. (2016) reported on the electrochemical behavior and corrosion resistance of glassy Fe68.6-Ni28.2-Mn3.2 (at%) specimens which were studied in different concentrations of HCl solutions. The results indicated that the corrosion rate increased with increasing concentration of the HCl solutions. Electrochemical impedance spectroscopy results were analyzed by fitting the experimental data to an equivalent circuit using the ZSim Demo program, and suitable equivalent circuit models were determined. The results obtained from the impedance and polarization measurements are in good agreement. The thermodynamic parameters were evaluated for the corrosion process and discussed. In order to further research in this novel area for better service condition, the present work has been undertaken.

**Research Methodology**

A spark plasma sintering machine (model SPS 10-3), manufactured by Thermal Technologies LLC, was used to produce the alloy samples. Specimens of diameter 100mm were produced using dies and punches of graphite. The samples were produced at a temperature of 11500C temperature and a pressure of 5MPa with heating and cooling rate of 100C/Min. the thermocouple inserted into the bottom punch was used to measure the temperature. All the samples were produced in a closed furnace where 10-2 torr vacuum was maintained throughout the experiment. A standard Ni-Fe base superalloy (INCONEL718) with composition shown in Table 1 below was used.

**Table 1: Composition of the superalloy INCONEL 718 used (wt%)**

| Ni | Fe | Cr | Mo | Mn | Si | C | Al | Ti | Other |
|---|---|---|---|---|---|---|---|---|---|
| 53 | 18.5 | 18.6 | 3.1 | 0.3 | 0.4 | 0.4 | 0.4 | 0.9 | 5.0 Co |

A carbolite furnace was used for the heat treatment of the samples. The samples were placed inside the furnace and the following heat treatment programme was used.

i. Hold at 1000C for 1 and 2 hours: then rapidly cool by quenching in water.
ii. Hold at 8000C for 1 and 2 hours; then air cool,

X-ray diffraction (XRD) analysis, with Cu-Kα radiation, was conducted using a PANalytical X'Pert PRO. The XRD was operated at 45KV voltage and 40mA current.

The 2 angles between 10 and 900 were scanned and analyzed using the Bragg Law. A Rietveld refinement software, TOPASTM was used for quantitative analysis. A TESCAN Scanning Electron Microscope was used in the research. The polished and etched samples were firmly held in the sample holder using a double-sided carbon tape before putting them inside the sample chamber. The SEM was operated at an accelerating voltage of 20 KV.

Electrochemical measurements were carried out using an Autolab potentiostat with the General-purpose Electrochemical Software package. The samples were cold mounted with epoxy leaving a working surface was ground with grinding papers from 600 to 1000 grit, and then cleaned with the distilled water and ethanol. A conventional three electrode cell, consisting of Ag/AgCl, Platinum and samples was used as: reference, counter and working electrodes respectively. The medium used for the electrochemical measurement was 0.5MH2SO4. The measurement was carried out at room temperature. The potentiodynamic potential scan was fixed from -1.5 V to +1.5 V with a scan rate of 0.012 V/s.

**Results and Discussion**

Figure 1a shows the XRD pattern of the untreated alloy, while Figures 1b-1e display the XRD patterns of the heat-treated samples. From the XRD spectrum of the alloy, it is observed clearly that there is presence of Ni, Fe (Awaruite), AL0.3Fe3 Si0.7 (Aluminum iron Silicon), and Cr7C3 (carbon Chromium) phases. After heat treatment it is observed that new phases appeared such as: FeSi (Fersilicite, syn [NR]), Managnese Carbide, Chromium Iron Carbide, Managanese Silicon Carbide. The presence of (Ni, Fe) (Awaruite) phase is common to all the samples; this expected because the specimen is a Ni-Fe base superalloy. By comparing the XRD of the control (Figure 1a) with the heat-treated samples (Figures 1b- 1e), one can observe that there is a great change in the spectrum which resulted in more diffraction peaks, and a larger quantity of hard carbides with smaller inter-particle distance. In the heat-treated samples, it is clear that the various phases formed after the heat treatment depends on the heat treatment condition as shown in Table 2.

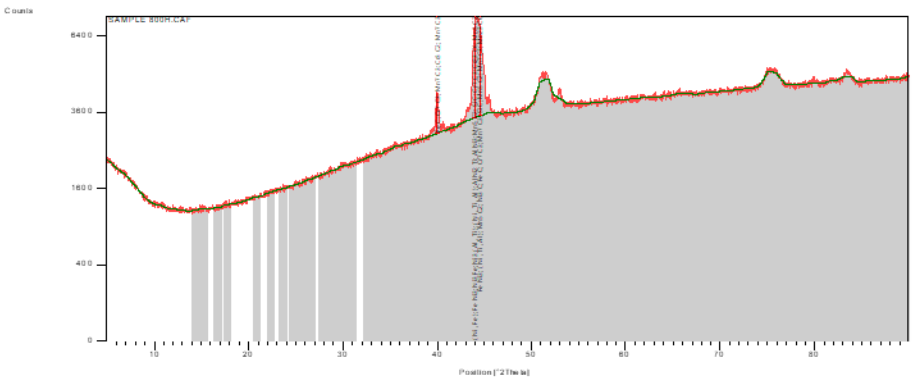

**Figure 1a: XRD spectrum of the untreated alloy**

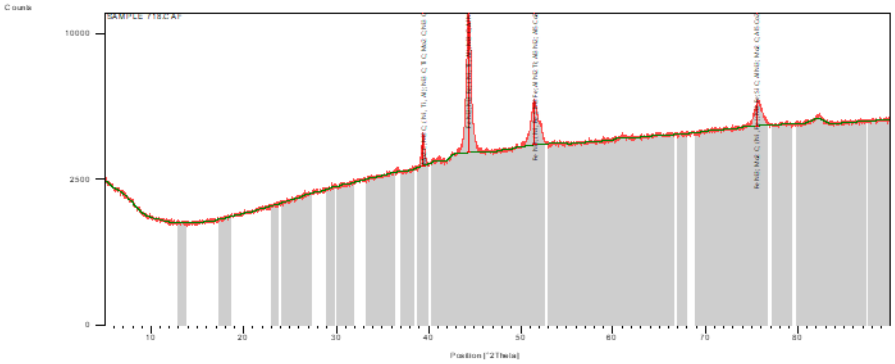

**Figure 1b: XRD spectrum of alloy heat treated at HT10001hr**

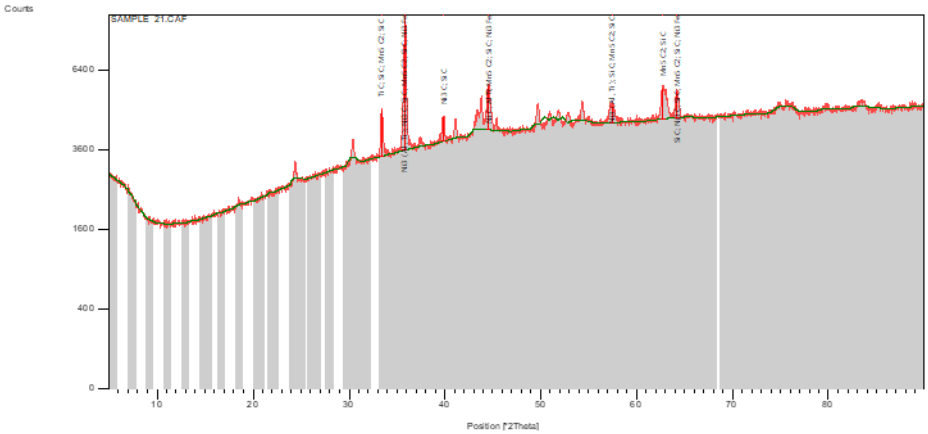

**Figure 1c: XRD spectrum of alloy heat treated at HT10002hrs**

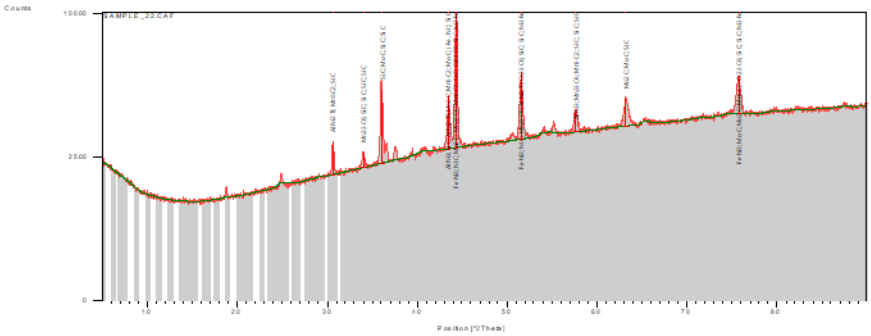

**Figure 1d: XRD spectrum of alloy heat treated at HT8001hr**

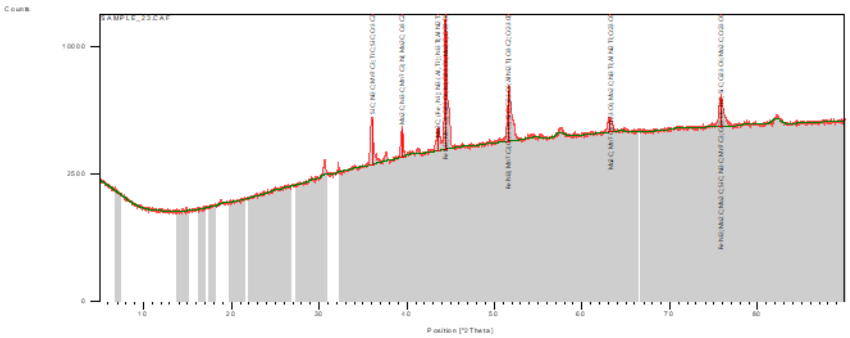

**Figure 1e: XRD spectrum of alloy heat treated at HT8002hrs**

Table 2: Identified patterns list

| Control | HT10001HR | HT10002HR | HT8001HR | HT8002HR |
|---|---|---|---|---|
| `(Ni, Fe) (Awaruite) | (Ni,Fe) (Awaruite) | Ni,Fe) Awaruite) | Ni,Fe) Awaruite) | Al Cr Fe2 |
| Al0.3 Fe3 Si0.7 (Aluminum Iron Silicon) | Mn5 c2 (Manganese Carbide) | Al Ni2 Ti (Aluminum Nickel Titanium | Fe Si(Fersilicite, syn [NR]) | Fe Si(Fersilicitie, syn [Nr]) |
| Cr7C3 (Carbon Chromium) | Al0.5 Fe0.5 (Aluminum Iron) | Al0.96 Ni1.04 (Aluminum Nickel) | C0.12 Fe0.79 Si0.09 (Carbon Iron Silicon) | Fe Ni3 (Awaruite) |
| Ni3 (Al, Ti) (Udimet 500') | Mn Si (Manganese Silicon) | Fe7 C3 (Iron Cabide) | Fe3 C (Cementite) | Ni2 Si (Nickel Silicon) |
| | (Cr, Fe)7 C3 Chromium iron Carbide) | Al0.4 Fe0.6 (Aluminum Iron) | Cr3 Ni2 (Chromium Nickel) | Mn 15C4 (Manganese Carbide) |
| | Ni2.67 Ti1.33 (Nickel Titanium) | Cr22 C6 (Carbon Chromium) | Al2 Ti (Aluminum Titanium) | (Cr, Fe)7 C3 (Chromium Iron Carbide) |
| | Mn22.6 Si5.4 C4 (Manganese Silicon Carbide) | | Ni74 Si26 (Nickel Silicon) | |

From the Figures 2a-2e, one can observe a great difference between the morphology of the untreated alloy (see figure 2a) and those of the heat-treated samples (see figures 2b-2e). Samples heat treated for 1 hr have a more refined structure. The dark spots show the presence of some of the new phases developed during heat treatment.

The electrochemical potential of the alloy was investigated using H2SO4 solution. Table 3 presents the corrosion data including the corrosion rate, while Fig 3(a) and 3 (b) present results of the polarization tests. From the results obtained in Table 3 and Figure 3, the corrosion rate of the sample generally decreases after heat treatment. The untreated sample has the higher corrosion rate. This was attributed to the high anodic potential reached by the sample. Meanwhile, as the sample was heat treated there was decrease in corrosion rate. This may be attributed to the formation of a hard-thin film, which may have retarded the ingress of SO4-2 ions. As the heat treatment time decrease from 2 to 1 hr the corrosion rate of the alloy decreased. Heat treatment contributes immensely to the corrosion behavior of the alloy (see Figure 3) E.g Corrosion rates of 2.55 (untreated), 1.302, 3.59, 1.835 and 1.14mm/year were obtained for samples heat treated at 10000C for 1, 2hrs and 8000C for 1, 2hrs respectively. The various hard phases formed after heat treatments are the major factor responsible for the improvement in the corrosion behavior of this alloy.

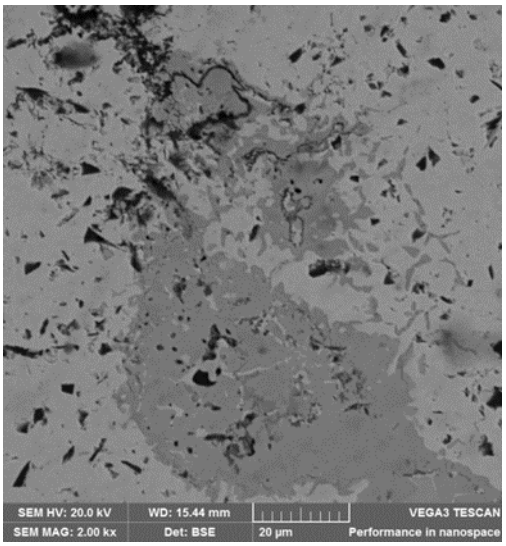


Figure2a: SEM image of untreated alloy

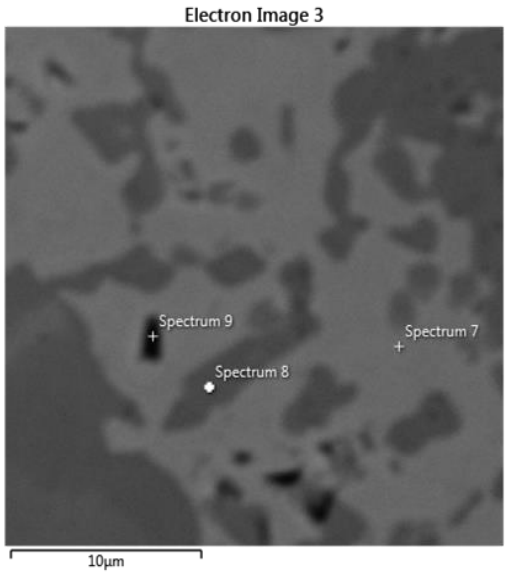


Figure 1b: SEM image of alloy heat treated at HT10001hr

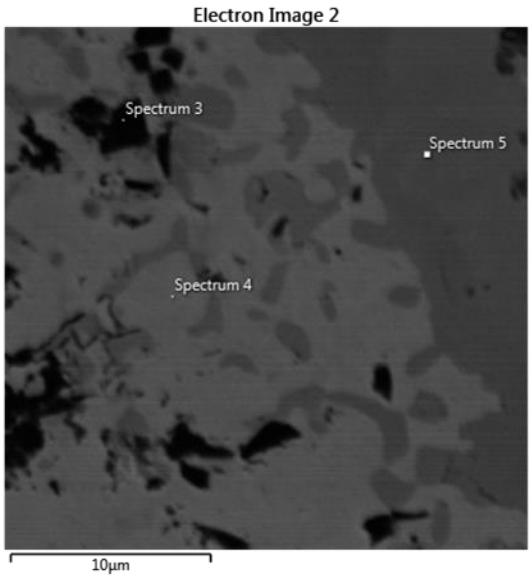


Figure 2c: SEM image of alloy heat treated at HT10002hrs

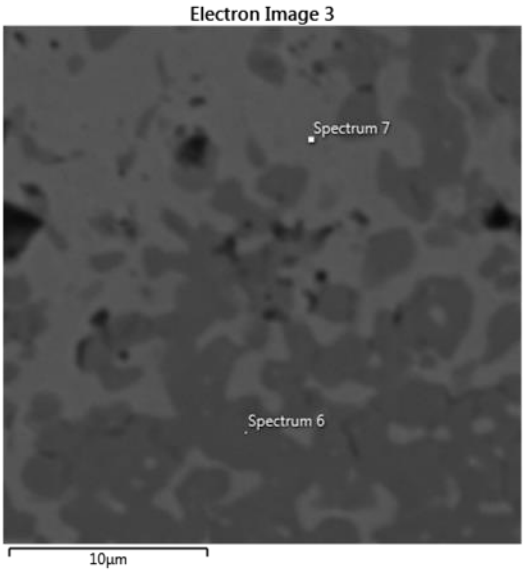


**Figure 2e: SEM image of alloy heat treated at HT8002hrs**

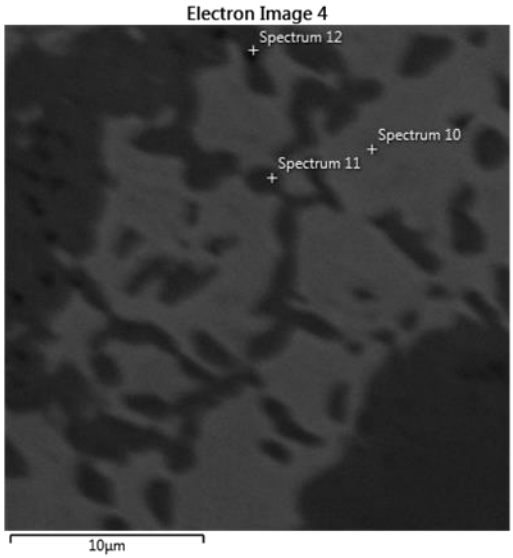


**Figure 2d: SEM image of alloy heat treated at HT8001hr**

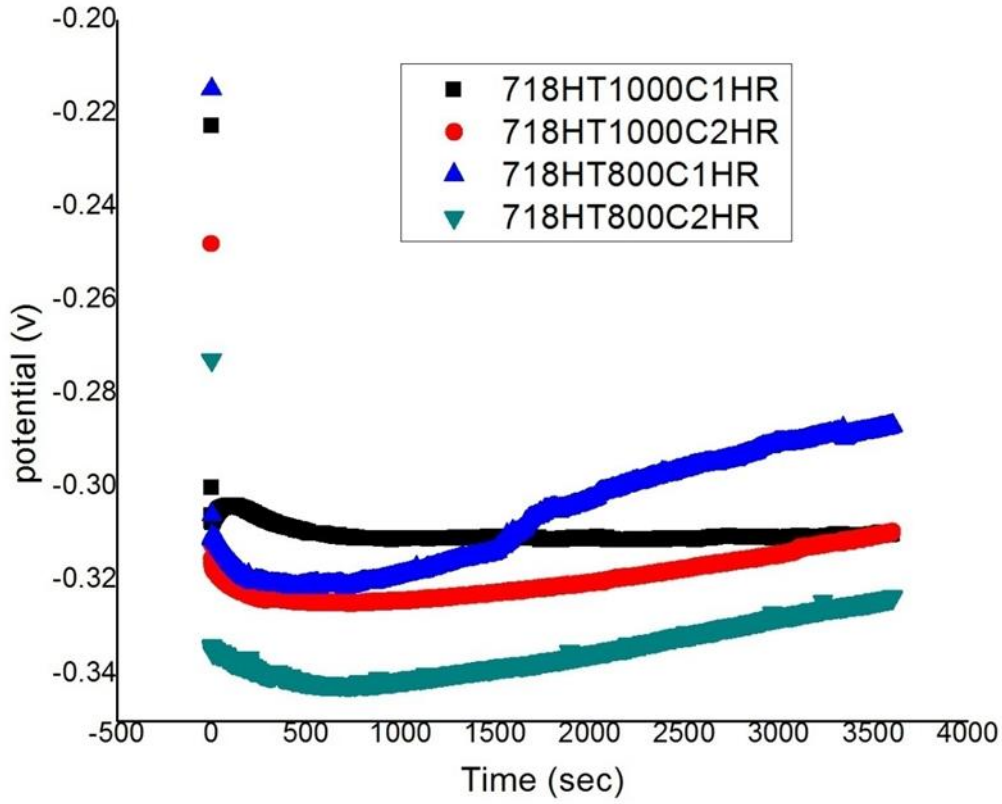


**Figure 3a: Variation of open circuit potential with time**

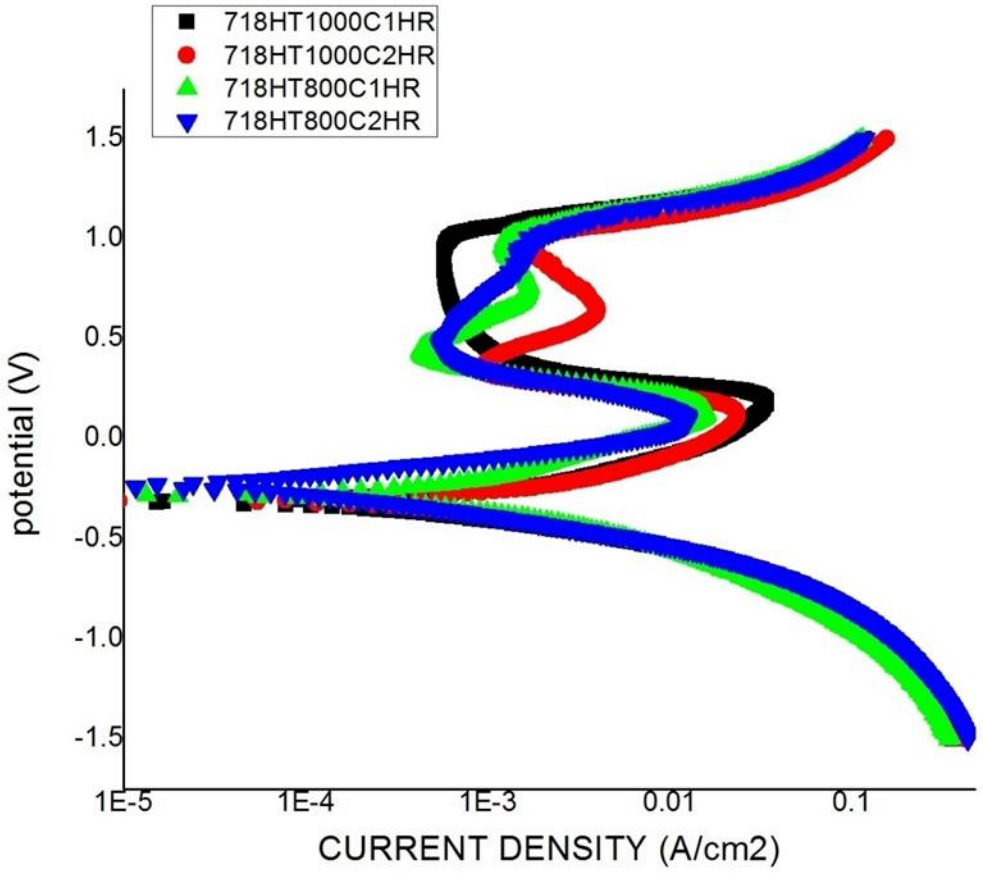

**Figure 3b: Potentiodynamic Polarization Curve**

**Table 3a: Electrochemical corrosion data**

| SAMPLE | $E_{corr}$ | $I_{corr}$(A/cm2) | $R_p$(Ω) | $\beta_a$(V/dec | $\beta_c$(V/dec) | CR(mm/Y) |
|---|---|---|---|---|---|---|
| Control | -0.359 | 2.35E-04 | 1.69E+01 | 0.064 | 0.112 | 2.55E+00 |
| 718HT1000C1HR | -0.316 | 1.199E-4 | 2.264E+1 | 0.059 | 0.083 | 1.302E+0 |
| 718HT1000C2HRS | -0.309 | 3.31E-04 | 1.71E+01 | 0.08 | 0.128 | 3.59E+00 |
| 718HT800C1HR | -0.366 | 1.708E-4 | 1.62E+1 | 0.054 | 0.093 | 1.853E+0 |
| 718HT800C2HRS | 0.279 | 1.05E-04 | 7.25E+01 | 0.113 | 0.122 | 1.14E+00 |

**Table 3b: Upper and lower levels used with their Corrosion Rate**

| S/No | Temperatures (A) 0C | Time (B) hrs | Corrosion rate (mm/yr) |
|---|---|---|---|
| 1 | 800 | 1 | 1.853E+0 |
| 2 | 1000 | 2 | 3.59E+00 |
| 3 | 1000 | 1 | 1.302E+0 |

The heat-treated sample may act as a cathode, which prevents conductance of ions but allows electronic conductance to some extent. It should also be emphasized that the electrical potential in all the samples decreases in the direction from the anode to the cathode (positive ions move towards the cathode, negative ions towards the anode (see Figures 3a). The surface of the anode in reality is much smaller than that of the cathode; i.e. the electrolytic current density is much higher near the anode. It is worthy to note in this present work that heat treatment temperature and time play a vital role in the electrochemical potential of all the samples. The optimum condition that led to the higher corrosion resistance is the sample heat treated at HT8002hrs. This optimum condition gave a protection efficiency of 55.29%.

Two factors and level of factorial design experiment were used to study the influences of heat treatment temperature and time on the corrosion behaviour of the materials. Table 3b, shows the upper and lower level s of each variable with their response values. Figure 4, shows the estimated response surface for the samples. It is observed that the corrosion rate increases with increase in heat treatment temperature and time. For example, as the temperature increases from 800 to 10000C and the time from 1 to 2hours the corrosion rate increased rapidly (see figure 4). Equation 1 shows the dependence of corrosion rate on temperature and time.

Corrosion rate = 1.97125 + 0.47475* Temperature + 0.39375* Time (1)

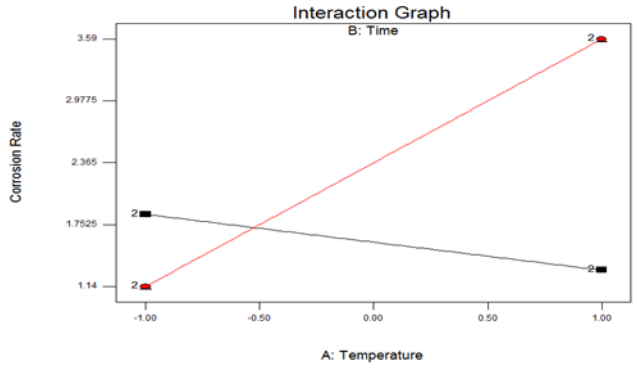

**Figure 4a: Interaction curve for the corrosion behavior**

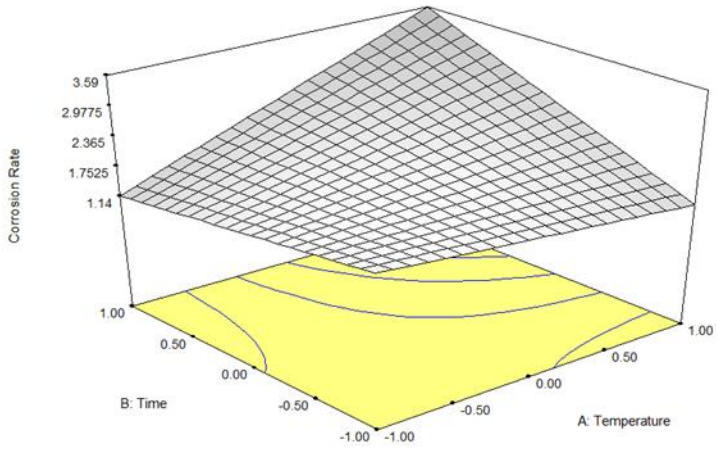


**Figure 4b: 3-D plot for the corrosion behavior of the 718 alloy**

From equation 1, it can be clearly seen that the coefficients associated with temperature and time are positive. It indicates that as the temperature rises from 800 to 10000C, the corrosion rate rises by 0.47475. Also, as the time increases from 1 to 2hours the corrosion rate rises by 0.39375. This further supports the earlier observation in figure 4a and 4b analysis of variance (ANOVA) was used to determine the design parameters significantly influencing the corrosion rate. Table 3b shows the results of ANOVA at 95% confidence level (significant level of $\propto$=0.05). The last column of table 3c shows the contribution (p) of each parameter to the response, indicating the degree of influence on the results.

The "Model F-value" of 0.34 implies the model is not significant relative to the noise. There is a 77.25 % chance that a "Model F-value" this large could occur due to noise. Values of ''prob > F'' less than 0.0500 indicate that the model terms are significant. In this case, A (Temperature) and B (time) are not significant model terms.

**Table 3c: ANOVA for selected factorial model**

| | | |
|---|---|---|
| Source | Sum of squares | DF |
| Model | 1.52 | 2 |
| A | 0.90 | 1 |
| B | 0.62 | 1 |
| Residual | 2.25 | 1 |
| Cor Total | 3.77 | 3 |

**Conclusion**

From the results and discussion above the following conclusions can be made:

1. The heat-treated alloy shows better corrosion resistance than the untreated alloy.
2. Heat treatment temperature and time have great influence on the corrosion behaviour and morphology of the alloy.
3. The sample heat treated at 800OC for 2 hours gave a high protection efficiency of 55.29%
4. It has been established that heat treatment can be used in improving the corrosion resistance of the alloy.

**References**

Calandri, M.; Manfredi, D.; Calignano, F.; Ambrosio, E.P.; Biamino, S.; Lupoi, R.; Ugues, D. (2018) Solution Treatment Study of Inconel 718 Produced by SLM Additive Technique in View of the Oxidation Resistance. *Adv. Eng. Mater*., 20, 1800351.

Deng, D.; Moverare, J.; Peng, R.L.; Söderberg, H. Microstructure and anisotropic (2017) mechanical properties of EBM manufactured Inconel 718 and e_ects of post heat treatments. *Mater. Sci. Eng. A,* 693, 151–163.

Hua, Y.; Liu, Z. (2018) Experimental Investigation of Principal Residual Stress and Fatigue Performance for Turned Nickel-Based Superalloy Inconel 718. *Materials*, 11, 879.

Khadiah M. Emran, (2015) Effects of concentration and temperature on the corrosion properties of the Fe-Ni-Mn alloy in HCL solutions. *Res Chem Intermed,* 41, 3583-3596

Li, L.; Gong, X.; Ye, X.; Teng, J.; Nie, Y.; Li, Y.; Lei, Q. (2018) Influence of Building Direction on the Oxidation Behavior of Inconel 718 Alloy Fabricated by Additive Manufacture of Electron Beam Melting. *Materials* 11, 2549.

Lin, Y.C.; Yin, L.-X.; Luo, S.-C.; He, D.-G.; Peng, X.-B. E (2018) ects of Initial _ Phase on Creep Behaviors and Fracture Characteristics of a Nickel-Based Superalloy. *Adv. Eng. Mater.,* 20, 1700820.

Locq, D., Walder, A; Marty, M; Caron, M.J. (2000) Development of New PM Superalloys for High Temperature Application EUROMAT, Intermetallics and Superalloys Vol. 10, WILEY-VCH Verlag Gmbh, Weinheim, Germany (D.G. Morris et. al., eds), 52-57.

Lyu, F.; Liu, F.; Hu, X.; Yang, X.; Huang, C.; Shi, D. (2019) The delta Phase Precipitation of an Inconel 718 Superalloy Fabricated by Electromagnetic Stirring Assisted Laser Solid Forming. *Materials*, 12, 2604.

Ma, W.; Xie, Y.; Chen, C.; Fukanuma, H.; Wang, J.; Ren, Z.; Huang, R. (2019) Microstructural and mechanical properties of high-performance Inconel 718 alloy by cold spraying. *J. Alloys Compd.*, 792, 456–467.

Moussaoui, K.; Rubio, W.; Mousseline, M.; Sultan, T.; Rezai, F. E. (2018) _ects of Selective Laser Melting additive manufacturing parameters of Inconel 718 on porosity, microstructure and mechanical properties. *Mater. Sci. Eng. A*, 735, 182–190.

Nunes, R.M.; Pereira, D.; Clarke, T.; Hirsch, T.K (2015) Delta Phase Characterization in Inconel 718 Alloys ThroughX-ray Di_raction. *ISIJ Int.,* 55, 2450–2454.

Paula Rojas, Rosa Vera, Carola Martinez, Maria Villaroel (2016) Effect of the Powder Metallurgy manufacture Process on the Electrochemical Behaviour of Copper, Nickel and Copper Nickel Alloys in Hydrochloric Acid. *Int. J. Electrochem. Sci.*, 11, 4701-4711.

Sano, K.; Oono, N.; Ukai, S.; Hayashi, S.; Inoue, T.; Yamashita, S.; Yoshitake, T. (2013) -Ni3Nb precipitate in Fe–Nibase alloy. *J. Nucl. Mater*., 442, 389–393.

Soucail, M.; Marty, M; Octor H. (1996) Development of Coarse Gran Structures in a Powder Metallurgy Nickel Base Superalloy N18. *Scripta Mater*, 34(4), 519-525.

Viswanathan, G.B.; Sarosi, P.M.; Henry, M.F; Whitis, D.D.; Milligan, W.W.; Mills, M.J. (2005) Investigation of Creep Deformation Mechanisms at Intermediate Temperatures in Rene 88 DT. *Acta Mater*, 53, 3041-3057.

Wesley, W.A. and Copson H.R. (2018) Effect of Non-Condensable Gases on Corrosion of Nickel in Steam Condensate, *TRANS. ELECTROCHEM. SOC.*,May, 1949.

Wlodek, S.T. Kelly, M; Alden D. (1992) The Structure of N18 Superalloys 1992 TMS, Warrendale, PA, U.S.A (S.D. Antolovich et al., eds), 467-476.

Zhang, H.; Li, C.; Guo, Q.; Li, H.; Liu, Y. (2018) Deformation Mechanism of L12-0 Phase in Bimodal -0Precipitation Hardened Inconel 718 Superalloy. *Adv. Eng. Mater.,* 20, 1800652.

Zhang, H.; Li, C.; Liu, Y.; Guo, Q.; Huang, Y.; Li, H.; Yu, J. E (2017) ect of hot deformation on and _ phase precipitation of Inconel 718 alloy during deformation & isothermal treatment. *J. Alloys Compd.*, 716, 65–72.